energies

MDPI

Article

Resonant Mechanism for a Long-Distance Wireless Power Transfer Using Class E PA and GaN HEMT

Ching-Yao Liu [1], Chih-Chiang Wu [2], Li-Chuan Tang [1], Yueh-Tsung Shieh [1], Wei-Hua Chieng [1,*] and Edward-Yi Chang [3]

[1] Department of Mechanical Engineering, College of Engineering, National Yang-Ming Chiao-Tung University, Hsinchu 30010, Taiwan; liucy721.me09g@nctu.edu.tw (C.-Y.L.); newton4538.eo85g@nctu.edu.tw (L.-C.T.); onion0720.me09g@nctu.edu.tw (Y.-T.S.)

[2] Mechanical and Mechatronics Systems Research Laboratories, Industrial Technology Research Institute, Hsinchu 31040, Taiwan; john.wu@itri.org.tw

[3] Department of Material Science and Engineering, College of Engineering, National Yang-Ming Chiao-Tung University, Hsinchu 30010, Taiwan; edc@mail.nctu.edu.tw

* Correspondence: cwh@nycu.edu.tw; Tel.: +886-3571-2121 (ext. 55152)

Abstract: This paper presents a study on long-distance wireless power transfer (WPT), which formulates the voltage gain in terms of the coupling coefficient between the power transmitting unit (PTU) and the power receiving unit (PRU) coils. It is proposed that maximum power transfer efficiency (PTE) can be reached when maximum voltage gain is achieved under a matching condition between the coil quality factor and the coupling coefficient. In order to achieve maximum power delivered to load (PDL), we need to elevate the input voltage as high as the high breakdown-voltage of gallium nitride (GaN) high-electron mobility transistors (HEMT) along with class E amplifier circuit topology. In order to promote voltage gain, knowledge of the coupling coefficient between two coils including the factors of the coil diameter, wire diameter, coil turns, and the coil resistance are derived. It was observed that a lower coil resistance leads to a reduced parallel quality, which facilitates long-distance wireless power transfer. Experimental results support the findings that the maximum PTE occurred at the maximum voltage gain existing at a specific distance matches the coupling coefficient between coils. A maximum power point tracking (MPPT) method is also developed to achieve maximum PDL. At a distance of 35 cm, experiments with more than 100 W successfully receive a PTE of 57% at the PRU when the received voltage reached 1.4 kV. This is used to verify the concepts and analysis that are proposed in this paper.

Keywords: voltage gain; coupling coefficient; resonant wireless power transfer; class E power amplifier (PA); GaN

Citation: Liu, C.-Y.; Wu, C.-C.; Tang, L.-C.; Shieh, Y.-T.; Chieng, W.-H.; Chang, E.-Y. Resonant Mechanism for a Long-Distance Wireless Power Transfer Using Class E PA and GaN HEMT. *Energies* **2023**, *16*, 3657. https://doi.org/10.3390/en16093657

Academic Editors: Julien Buckley, Matthew Charles and René Escoffier

Received: 3 March 2023
Revised: 18 April 2023
Accepted: 21 April 2023
Published: 24 April 2023

1. Introduction

Wireless power transfer (WPT), due to its convenience and safety, has gained more attention and study [1–7]. An overview of resonant circuits for WPT systems and some key issues including the zero-voltage switching, zero-voltage derivative switching, and total harmonic distortion are addressed in [1]. Moreover, the classification of wireless power transfer, its application, trends, advantages, and disadvantages are presented in [2]. WPT enables efficient wireless charging by decreasing battery size and improving convenience, therefore the application of WPT has been widely adopted for various domains such as electric vehicle (EV) charging [3,4], unmanned aerial vehicle (UAV) charging [5], and implantable medical devices [6]. In [3], a comprehensive overview of recent trends in WPT technologies and applications of the wireless charging of EVs are presented, and the latest technologies of WPT to charge EVs are investigated in [4]. Furthermore, a wireless power transmission system via inductive coupling and the power efficiency of the inductive coupling are analyzed in [5]. In [6], the various strategies implemented for

WPT are reviewed in implantable medical devices, and a systematic review is presented based on the system design and optimization methodology. Among the resonant circuits in WPT systems, the class E circuit is one of the simple topologies equipped with high efficiency under zero voltage switching (ZVS) and zero voltage derivative switching (ZVDS) conditions, which makes it widely used in the WPT systems [1,7].

When it comes to the high efficiency and high transmission power capability of the WPT, the coupling coefficient, the power evaluation from the induced electromagnetic field of the secondary coil, is an important parameter that is used to maintain better coupling efficiency [7,8]. Nevertheless, the coupling coefficient can be affected due to the winding of the antenna, the variation distance of the coils, and the difference of the angle [8]. In [9], the impact of the coupling coefficient k implemented on the passive clamp coupled inductor Boost converter is investigated, and shows that the dc voltage gain is negatively affected by the coupling coefficient and the output current. Hence, for achieving a better understanding, the coupling coefficient induces the operation of the coupled inductor converters. An extension of the work is presented in [10]. In addition, the low- and mid-frequency model of the transformer with a resistive load for different values of coupling coefficients is analyzed in [11], in which the voltage gain, current gain, bandwidth, input impedance, and transformer efficiency can be derived based on the coupling-dependent inductances model. Previous studies have explored the use of multilevel coils in WPT systems [12–14] to enhance coupling efficiency. In [12], an algorithm was proposed for optimizing energy computation. In [13], a dual-frequency dual-load WPT system was utilized for PRU power sharing. The work in [14] introduced a dynamic magnetic coupled (MC) WPT system that leveraged the compensation of multiple coils to maintain stable mutual inductance, resulting in high PTE.

Previous studies have analyzed the behavior of the coupling factor as a function of the variation between the critical parameters of the coils. Rafael Duarte et al. proposed a simple equation using Neumann's equation for mutual inductance to estimate the coupling coefficient between the coils [15]. Chabalko et al. derived an analytic expression for the coefficient between the fields in the cavity and a loop receiver [16]. For long distance and large power transmission, a large transmitter and receiver needs to be designed. A scaling law [17], which relates the coil size to the coupling coefficient, is proposed to estimate the efficiency of the large coil based on the results of the small coil for reducing the cost and effort required in the early stage of the work. To get a better WPT performance, a few methods [18–22], such as superconductor materials [18], strongly coupled magnetic resonance (SCMR) [19], compensation techniques [20], and three-resonator WPT systems [21] have been proposed. In [18], superconductor coils were used in WPT system and improved the PTE. In [19], SCMR was used to transfer 60 watts with merely 40% efficiency over distances more than 2 m. Coil wire resistance that results in ohmic losses affects the resonance frequency and efficiency, and a series compensation is used to reduce the influence of the coupling on the resonance frequency [20]. In [21], the concise formulas are derived to improve the PTE and PDL. The use of compensation coils in a three-stage WPT system to improve the transfer distance has been explored in previous research [22]. One commonly used topology for driving high-frequency WPT systems is the class E PA, as evidenced in studies [23–27]. The push-pull class E2 circuit [23] and the parity-time based class E2 circuit [24] have been utilized to achieve power transfer under high PTE conditions. Furthermore, parallel topologies have enabled the transfer of hundreds of watts of power with ease. To ensure stable output power in the face of load fluctuations, a design procedure for class E-based WPT systems was proposed [25]. Additionally, an impedance matching circuit for class E-based WPT systems was presented to maintain the PTE, even as the transfer distance changes. In our previous works, the ZVS control has been derived in terms of the resonant frequency and duty cycle, and the experiments show the agreement with the derivation of the ZVS control [7]. Furthermore, the minimum power input control that generates a look-up table has been presented to yield good power transfer efficiency in WPT applications [7]. High efficiency WPT is then achieved by using the resonant design for tuning resonant frequencies and duty cycles [27]. Moreover, a compatible charge pump gate driver has been designed to fully exploit the advantages of a fabricated GaN high electron mobility transistor (HEMT) in class E amplifiers [27–30]. In addition, a voltage-controlled oscillator (VCO) of radio frequency and capacitor-coupled difference amplifiers has been used to simultaneously tune the frequency and duty cycle for the efficiency requirement in resonant WPT applications [31]. For the further improvement of the resonant WPT system, the relationship between the resonant quality factor and the coupling coefficient are studied in this paper. Table 1 summarizes the resonant WPT system work done previously and shows that analyzing the relationship among the transfer distance, the frequency, and the receiving power is necessary, which is the key factor for long-distance WPT.

Table 1. Comparison of the resonant WPT system undertaken previously.

Ref.	WPT Distance	Frequency (MHz)	Receive Power	Technique	Coil Configure	Efficiency
[5]	4 cm	0.162	66 W	Resonant	Flat	62%
[13]	25 cm	0.34/0.44	12.5 W	Six-coil MC	Flat	68.6%
[17]	45 cm	1.97	1.4 W	Three-Resonator	Solenoid	33%
[18]	160 cm	9.14	N/A *	Resonant	Flat	49.7%
[19]	200 cm	0.9	60 W	SCMR	Solenoid	40%
[25]	N/A *	3.39	40 W	Three-Resonator	Solenoid	83.3%
[32]	7.6 cm	0.96	40 W	Resonant	Solenoid	50%
[33]	10 cm	10/20	N/A *	Resonant	Flat	48/46%

*: not applicable.

The goals of this paper include delivering more power in a fixed distance or delivering the same power to a longer distance. Both goals are associated with the quality factor of the parallel RLC that matches the optimal coupling coefficient, and involves the optimization of the coils' configuration of the WPT system to obtain the desired parallel quality factor. The paper is organized as follows. Section 2 analyses the constant product of the voltage gain and the coupling coefficient, which is subdivided into a discussion on the inductor for WPT, the transmitter and receiver voltage analysis of the WPT, the derivation of the voltage gain with the assumptions, and the power analysis. Section 3 describes the WPT transformer analysis, which includes a brief introduction of the external inductance, the optimal configuration of the transformer, the limitation on the wire diameter, and the coil design examples which will be used in the experiments. Section 4 describes the coupling coefficients regarding Section 3 and the class E PA and experimental results obtained to verify the proposed findings. The conclusions and extension work of the wireless power transfer applications that could benefit from the present work are presented in Section 5.

The core innovation of this paper regards the matching of the magnetic coupling coefficient to the resistance of the load on PRU when the resonant WPT is applied. We therefore need to know the function of the coupling coefficient in terms of the coil radius, the coil radius, as well as the gap distance between the PTU and PRU. From the coupling coefficient, we then calculate the exact quantity of the load resistance for the maximum power transfer when the distance gap is given. The MPPT method can then be achieved via the load resistance tuning to track the maximum power received by the PRU. The term MPPT is borrowed from the solar PV technology [34], and the control such as the hill climbing method can be performed in the future when the PRU is moving.

2. Constant Product of Voltage Gain and Coupling Coefficient

2.1. Inductor for WPT

Since the WPT does not have a magnetic core, the equivalent circuit of the wireless transformer can be obtained by removing the core-loss resistance, which is parallel with the magnetization inductance L_m from the general version of the transformer [10,11,16]. The Steinmetz equivalent circuit is shown in Figure 1, where v_T and v_R is the voltage across the transmitter coil and receiver coil, R_T is the reluctance, $L_{T,s}$ is the self-inductance, $L_{R,l}$ is the leakage inductance on the receiver coil, $R_{R,c}$ is the coil resistance, C_R is the resonant capacitor, Z_o and Z_R represent the load impedance and the receiver impedance, respectively, N_T and N_R are the coil turns of the transmitter coil and receiver coil. The mutual inductance L_m is related to the transfer voltage $v_{T,i}$ by the equation, as follows.

$$v_{T,i} = L_m \frac{di_{T,m}}{dt} = N_T \frac{d\varphi_m}{dt} \tag{1}$$

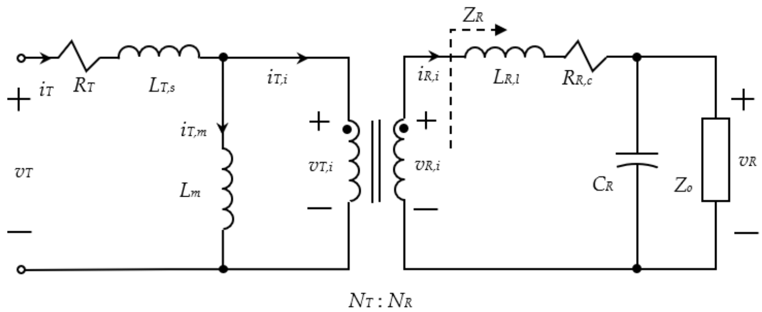

Figure 1. The equivalent circuit of the WPT.

The flux density B in the unit of Tesla is defined by three parts consisting of the magnetization flux φ_m, the ideal transformer induction flux φ_i, and the self-induction flux φ_s.

$$B = \frac{\varphi}{A} = \frac{\varphi_i + \varphi_m + \varphi_s}{A} \tag{2}$$

A is the cross-section area of the PTU inductor. The self-induction flux φ_s is assumed to be

$$\varphi_s = \frac{1-k}{k}\varphi_m \tag{3}$$

The above equation is valid only if φ_m goes through a PRU. Assuming that the induction flux went through the exact the path of the magnetization flux, the induction current on transmitter $i_{T,i}$ can be expressed as follows.

$$i_{T,i} = \frac{N_T \varphi_i}{L_m} = \frac{1}{a} i_R \tag{4}$$

i_R is the current flowing through the inductor of the PRU, and a is the turn ratio which satisfies $a = N_T/N_R$.

2.2. Transmitter and Receiver Voltage in WPT

The voltage $v_{R,i}$ can be written as

$$v_{R,i} = \frac{L_m}{a}\frac{d\varphi_i}{dt} = \frac{1}{a} v_{T,i} \tag{5}$$

The transmitter voltage v_T on the PTU assuming $R_T = 0$ is

$$v_T = L_{T,s}\frac{di_T}{dt} + L_m \frac{di_{T,m}}{dt} = N_T \left(\frac{d\phi}{dt} + \frac{1-k}{k}\frac{d\phi_i}{dt} \right) \tag{6}$$

Substituting Equations (1), (4) and (5) into (6), we have

$$v_T = \frac{a}{k} v_{R,i} + \frac{1-k}{a} L_T \frac{di_{R,i}}{dt} \tag{7}$$

The first term involving the induced receiver voltage $v_{R,i}$ on the right hand side of the above equation is the inductive part of the WPT. The second term involving the time derivative of the induced receiver current $di_{R,i}/dt$ is the resonant part of the WPT. Equation (7) explains that the transmitter voltage v_T needs to produce a higher voltage to account for the inductive part when the receiver is at a longer distance, and the same induced receiver voltage $v_{R,i}$ as the coupling coefficient reduces at a rapid rate according to the distance. The resonant part of the transmitter voltage is a function of the magnitude of the receiver i_R. The phase of the resonant part, is theoretically at a 90° lag from the induced receiver voltage $v_{R,I}$, when the receiver is at an excellent quality factor of resonance. However, in reality, the quality factor can neither be infinite voltage nor be in zero current. With a small inductance L_T, the magnitude of the current needs not be very small for the same amount of transmitter voltage v_T. Regardless whether the distance between PTU and PRU is significant, the $1-k$ factor cannot affect the increasing distance, which becomes a reason for the resonant WPT to be useful at long distances.

As the receiver voltage v_R (including the leakage inductance and the coil resistance on the receiver) is directly measured from the winding of the PRU, the overall load impedance Z_R from the view of inductive voltage and leakage inductance on the receiver side becomes

$$Z_R = Z_O \Big|\Big| Z_{C_R} + Z_{L_{R,l}} + R_{R,c} \tag{8}$$

Z_{C_R} and $Z_{L_{R,l}}$ are the impedance of C_R and $L_{R,l}$ on the winding on the receiver side. A simpler way to measure the coupling coefficient is to have Z_o be the open circuit. Assuming the turn ratio, $a = 1$ for the following derivation, the transmitter and receiver voltage are expressed as follows

$$v_R = \mathrm{Re}\Big(V_R e^{j\omega_0 t}\Big) = \frac{Z_{CR}}{Z_R} v_{R,i} \tag{9}$$

$$v_T = \mathrm{Re}\left(V_R e^{j\omega_0 t}\Big(\frac{Z_R}{kZ_{CR}} + \frac{1-k}{Z_{CR}} L_T j\omega_0\Big)\right) \tag{10}$$

where ω_0 is the natural angular frequency. The impedance Z_R becomes

$$Z_R(\omega_0) = \Big(1 - (1-k)\omega_0{}^2 L_R C_R\Big) Z_{CR} + R_{R,c} \tag{11}$$

Since the capacitor C_R holds for the resonance, we can have $\omega_0{}^2 = 1/L_R C_R$, and the impedance from the above equation is as follows.

$$Z_R(\omega_0) = (k + jQ_p) Z_{CR} \tag{12}$$

where Q_p is the parallel quality factor defined as follows.

$$Q_p = \omega_0 R_{R,c} C_R = R_{R,c}\sqrt{\frac{C_R}{L_R}} \tag{13}$$

2.3. Voltage Gain beteween Transmitter and Receiver

We made the PTU and PRU with similar windings, $L_T = L_R$, and the magnitude voltage gain $|G_{V,1}|$ is derived as follows.

$$|G_{V,1}| = \frac{V_R}{V_T} = \frac{k}{\sqrt{k^4 + Q_p{}^2}} \tag{14}$$

Figure 2 shows the relation between coupling coefficient k and the voltage gain $|G_{V,1}|$ with C_R = 200 pF, L_R = 10 μH for different Z_o. For a coupling coefficient higher than 0.5, the $|G_{V,1}|$ approaches one. Certain resonance peaks are seen at some specific coupling coefficient k. The coupling coefficient is also a monotonic decreasing function of distance, which will be discussed in the following sequels.

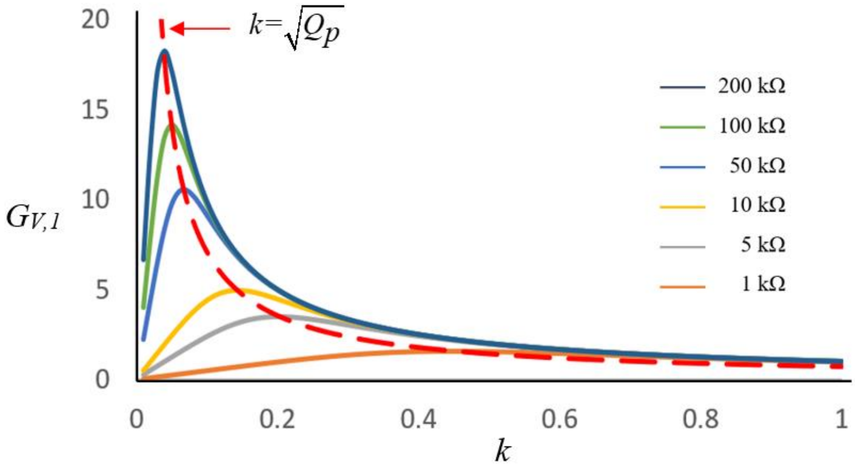

Figure 2. The voltage gain in terms of coupling coefficient for different load resistance Z_o when C_R = 200 pF and L_R = 10 uH.

On the other aspect, the resonance was not a perfect matching i.e., ${\omega_0}^2 = \psi_R / L_R C_R$ and also ${\omega_0}^2 = \psi_T / L_T C_R$, where ψ_R and ψ_T are the correction factor for receiver and transmitter. The Z_R is then becomes as follows

$$Z_R(\omega_0) = \left(k + (1 - \psi_R)(1 - k) + jQ_p\right) Z_{CR} \tag{15}$$

The correction factor ψ remains constant for fixed coil resistances, inductors and capacitors in the WPT circuit when the switching frequency is also fixed. The transfer function between the receiver and the transmitter is

$$G_{V,\psi} = \frac{V_R}{V_T} = \frac{k}{f(k) + jQ_p} \tag{16}$$

$$f(k) = \psi\left(k^2 + \varepsilon k - 1\right) + 1 \tag{17}$$

where the mismatch of the inductance $\varepsilon = 1 - L_T / L_R$ and $f(k)$ is a monotonic increasing function with the coupling coefficient k. The voltage gain can also be expressed as follows

$$\begin{cases} \left|G_{V,\psi}\right| = \dfrac{k}{\sqrt{f(k)^2 + {Q_p}^2}} \\ \angle G_{V,\psi} = -\tan^{-1}\dfrac{Q_p}{f(k)} = \begin{bmatrix} 0^\circ \ f(k) >> Q_p \\ -90^\circ \ f(k) << Q_p \end{bmatrix} \end{cases} \tag{18}$$

The phase is 0° when $f(k) >> Q_p$ and is -90° when $f(k) << Q_p$, which concludes that when the transformer is in the induction mode of the inductive wireless power transfer, the phase of the transfer function $G_{V,\psi}$ is 0°. Subsequently, when the transformer is in the resonant mode of the inductive wireless power transfer, the phase of the transfer function $G_{V,\psi}$ is -90°. Since the function $f(k)$ is a monotonic increasing function with the coupling coefficient k, we can also say that the short distance of the wireless power transfer will make $f(k)$ to be large and provide inductive power transfer energy. With the long-distance wireless power transfer, we are getting the resonant one. The stationary condition $\partial\left|G_{V,\psi}\right| / \partial k = 0$ with respect to the coupling coefficient is used to solve the optimal coupling coefficient k_{opt}. In the case that $\psi \approx 1$ and $\varepsilon = 0$, i.e., $f(k) = k^2$ in (14), the k_{opt} is derived as follows.

$$k_{opt} = \sqrt{Q_p} \tag{19}$$

The corresponding maximum voltage gain $G_{V,1}$ is related to the parallel quality factor as follows.

$$|G_{V,1}|_{\max} = \frac{1}{\sqrt{2Q_p}} \tag{20}$$

In the perfect resonance case, the voltage gain and coupling coefficient product is a constant, as follows.

$$|G_{V,1}k_{opt}|_{\max} = \frac{1}{\sqrt{2}} \tag{21}$$

Ideally, when the superconductor winding is available, we can send power with infinite voltage gain to the infinite space where the coupling coefficient reaches zero. We can also say that the highest wireless power transfer is definitely not the inductive mode and must be the resonant mode. However, it is very different from the far field electromagnetic wave (or radio wave) theory, and that the resonant wireless power transfer indeed utilizes a magnetic flux linkage which is known as the near field mechanism.

2.4. Analysis of Transmitted Power and Efficiency

Given that the antennas are made of copper coils and the conditions $\psi \approx 1$ and $\varepsilon = 0$ are difficult to achieve, the rule of thumb for the design optimization is to make $f(k)$ approach zero for the selected k, which is a function of coil distance. Nevertheless, the parallel quality factor must be reduced to a small value in order to increase the voltage gain. The condition $f(k) = 0$ can easily be achieved by adjusting ψ as follows.

$$\psi = \frac{1}{1 - k^2 - \varepsilon k} \tag{22}$$

Equation (22) is introduced to the switching frequency so that

$$\omega_0{}^2 = \frac{1}{(1 - k(k + \varepsilon))L_T C_R} \tag{23}$$

In accordance with (23), the switching frequency shall be a bit lower than the natural resonant frequency of the receiver LC tank. Where the purely resistive output impedance $Z_o = R_0$ is also concerned, it must comply with the series to parallel quality factor mapping in the resonance state, as follows. The output resistance R_0 is equivalent to the imposing of an extra coil resistance $\Delta R_{R,c}$ to the receiver winding, thus the parallel quality factor with load resistance $Q_{p,0}$ is derived as follows.

$$\begin{aligned} Q_{p,0} &= (R_{R,c} + \Delta R_{R,c})\sqrt{\frac{C_R}{L_R}} \\ \Delta R_{R,c} &= \frac{L_T}{R_0 C_R} \end{aligned} \tag{24}$$

The root mean square (RMS) output power $P_{0,RMS}$ is

$$P_{0,RMS} = \frac{\left(\frac{V_R}{\sqrt{2}}\right)^2}{R_0} = \frac{G_V{}^2 V_T{}^2}{2R_0} \tag{25}$$

The output resistance R_0 affects the parallel quality factor Q_p, and thus determines the distance where the maximum voltage gain is according to Equation (20). On the other hand, we can use some dc chopper or DC-DC converter controls to adjust the equivalent load resistance seen from the PRU [34].

Class E PA is one of the topologies used in the WPT system, as shown in Figure 3. The circuit has input voltage V_{DD}, input current I_1, the switching frequency $f_{,0}$ and the duty cycle δ; where L_1 is choke inductor, M_1 is a transistor, and C_T and L_T work as a resonant tank and also an impedance matching network. As the R_0 varies, the ZVS control can be implemented by change f_0 and δ. The purpose of the minimum power input control strategy [7] is used to optimize the power efficiency of the WPT system when the PTU and PRU are interacting. The control strategy calculates the optimal f_0, and δ for PTU with the following steps: (I) observing the voltage across the drain and source of M_1, achieving ZVS control by pulse frequency modulation (PFM); (II) observing the voltage across the drain and source of M_1, achieving ZVDS control by pulse width modulation (PWM). Thus, the required power will be limited to the minimum and achieve high efficiency simultaneously. The WPT PTE η_{WPT} is defined as

$$\eta_{\mathrm{WPT}} = \frac{P_{0,RMS}}{P_{in}} = \eta_{classE}\eta_{coils} \tag{26}$$

where P_{in} is the power input to class E PA, η_{classE} represents the power efficiency of the class E PA, and η_{coils} represents the efficiency of the coupling coils.

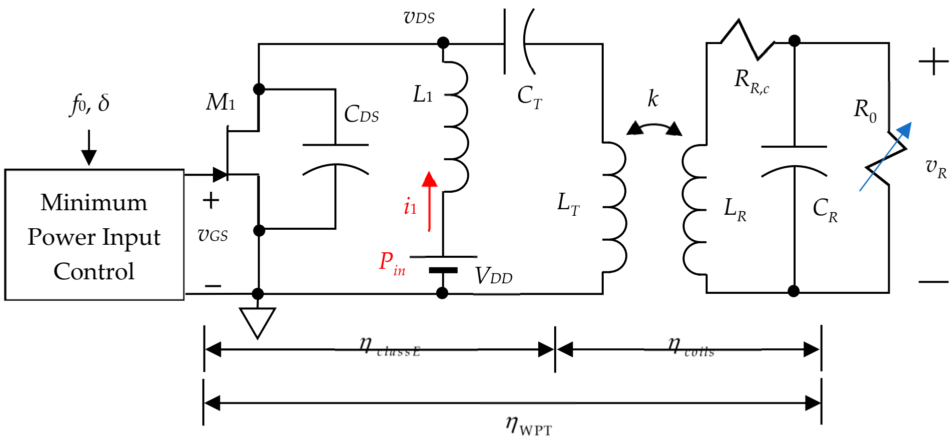

Figure 3. Topology of the resonant WPT system using Class E PA.

3. WPT Transformer Analysis

Designing and manufacturing a coil with low parasitic resistance and low inductance simultaneously is a challenging task [20]. In our findings, in order to obtain low Q_p, a low resistance coil is necessary; thus, the transferred power can be optimized. The constraint of the transformer design must include the inductance of the transformer coils to be confined into the range of several microhenry, as the resonant frequency of WPT in this paper is around 4 MHz, and the parasitic capacitance of the GaN transistor is around hundreds of picofarads. The parallel quality factor Q_p decreases with the larger wire diameter of the coil. However, the inductance of the transformer coils changes with the wire diameter of the coil when a helical coil is made [35,36]. It is then necessary to study the helical coil design to obtain the correct parameters of the helical coil for the same inductance. The actual inductance may also be shifted due to the fabrication process; thus, the inductances must be double checked and measured from the RLC meter after they are made.

3.1. External Inductance of Coil

Figure 4 exhibits the helical coil with the coil diameter D, coil length l in N turns, and the wire diameter d. The external inductance of the helical wire can be expressed as follows [36].

$$L_{ext} \equiv L_T = \mu_o \frac{\pi N^2 D^2}{4l}\beta \tag{27}$$

where β is a dimensionless factor in Nagaoka's form [17]. The flux density to current gain G, referred to as inductance gain, is defined as follows.

$$G \equiv \frac{L_T}{N_T \pi \mu_0 A} \tag{28}$$

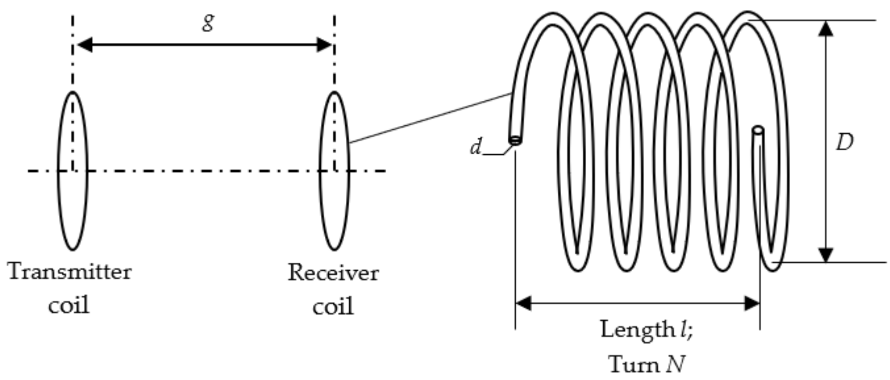

Figure 4. Parameter definition of helical coil.

The current sheet model, of which the wire diameter is infinitesimal, is assumed in the inductance analysis. The correction of the inductance due to the wire radius can be made in a later stage of the analysis. The helical coil is assumed to have a pitch equal to the wire diameter d. The form factor α is defined as follows.

$$\alpha \equiv \frac{l}{D} = \frac{Nd}{D} \tag{29}$$

The factor β in terms of form factor α is shown in Figure 5.

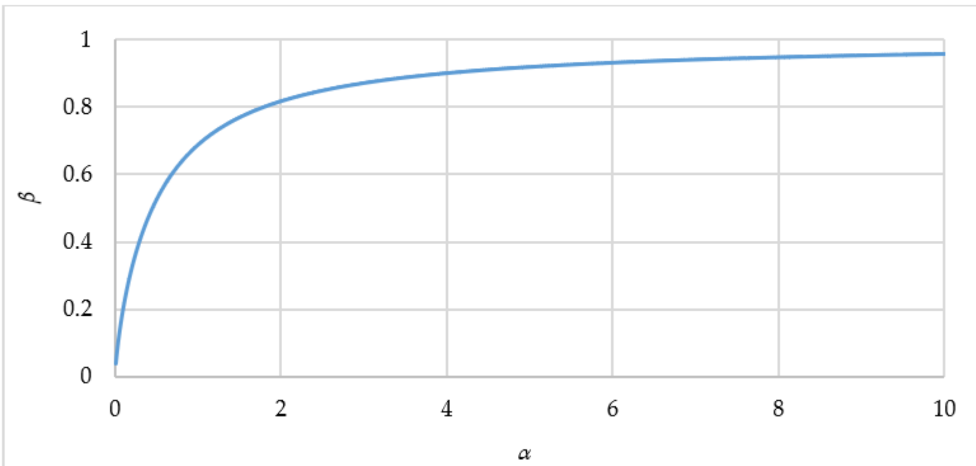

Figure 5. The factor β in terms of form factor α.

For a given inductance L_{ext}, the parameters may be calculated as follows.

$$N = \sqrt[3]{\frac{4\alpha^2 L_{ext}}{\mu_o \beta \pi d}} = \sqrt[3]{\frac{4L_{ext}}{\pi \mu_o d}}\gamma \tag{30}$$

$$D = \frac{\gamma}{G\pi}\sqrt[3]{\frac{4L_{ext}}{\pi \mu_0 d}} \tag{31}$$

where the dimensionless factor $\gamma = \sqrt[3]{\beta^2/\alpha}$ and μ_o is the permeability in the air.

According to Figure 6, $\gamma = 0.82$ is at around $\alpha = 0.4$ and the corresponding $\beta = 0.47$, which is considered as an optimal configuration for gain G. The wire length l_w is expressed by letting $N = N_T$, as follows.

$$l_w = N\pi D = \frac{4L_{ext}}{N\pi\mu_o} \tag{32}$$

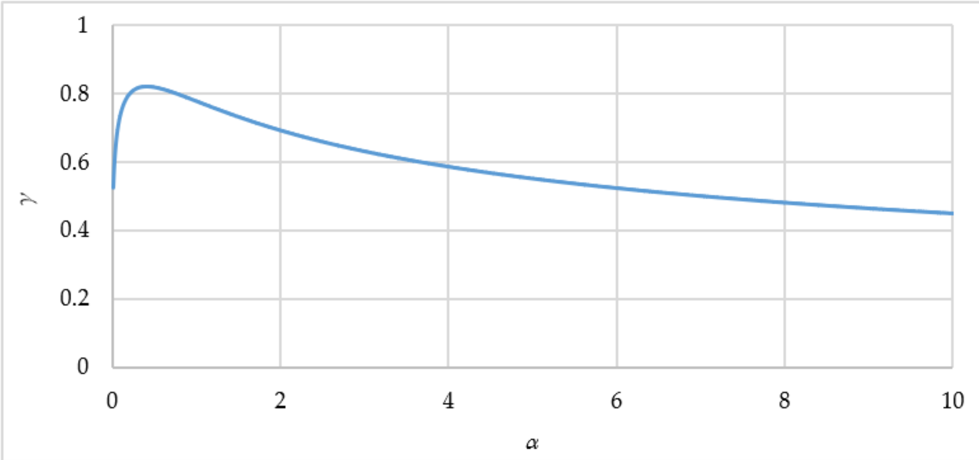

Figure 6. The factor γ in terms of form factor α.

Hence, according to (30) to (32), the coil can be precisely designed by acquiring coil turns, diameter and wire length from any parameter value D and L_{ext}.

3.2. Skin Effect on Wire Diameter

The conducting wire in the theoretical current-sheet is infinitely thin, and therefore has no internal inductance. Internal inductance is proportional to the wire length l_w, which is most likely to be significant in coils that have a low number of turns. The internal inductance of a wire at high frequencies is given by

$$\frac{L_{ext}}{l_w} = \frac{\mu_o}{2\pi}\frac{\delta_i}{d} \tag{33}$$

where the skin depth $\delta_i = \sqrt{\rho/\mu_i\pi f_0}$ is expressed in terms of frequency f_0 and μ_i, the permeability of the wire material. The skin effect made the current distribute on the surface of the coils; that is, higher the frequency, the lower the skin depth. The effect also made the conductor resistance high, which becomes a disadvantage for WPT.

3.3. Coupling Coefficient

The mutual inductance is given by Neumann's formula [15], and the coefficient k equation had been derived by Nagai [17]. Based on the assumption that two helical coils have the same diameter and the number of turns that are facing each other with the center axis aligned in the positional relationship, the k is then expressed as follows.

$$k = \frac{2l}{\mu_o\pi D}\frac{\varphi(x)}{\beta(\alpha)} \tag{34}$$

The $x \equiv x(g,l,D)$ is a function of the gap distance and the diameter, as follows, where l is ignored in Nagai's form. The gap distance g between two coils is redefined from the coil surface to the other coil surface, as shown in Figure 4.

$$x(g,l,D) = \sqrt{\frac{1}{1+\left(\frac{g+l}{D}\right)^2}} \tag{35}$$

where

$$\phi(w) = \frac{2}{w}(K(w) - E(w)) - xK(w) \tag{36}$$

$$K(w) = \int_0^{\pi/2} \frac{d\phi}{\sqrt{1 - w^2 \sin^2 \phi}} \geq \frac{\pi}{2} \tag{37}$$

$$\frac{\pi}{2} \geq E(w) = \int_0^{\pi/2} \sqrt{1 - w^2 \sin^2 \phi d\phi} \geq 1 \tag{38}$$

$$0 \leq w = \sqrt{\frac{1}{1+\alpha^2}} \leq 1 \tag{39}$$

Piri [35] considered the coil length and derived the coupling coefficient k equation as follows.

$$k = \frac{F(x(g+l,l,D)) - 2F(x(g,l,D)) + F(x(g-l,l,D))}{2F(x(g,l,D)) - 1} \tag{40}$$

Function F is a part of the Lorenz's expression [36] as follows.

$$F(w) = \frac{1}{w}\left(\frac{1-w^2}{w^2}(K(w) - E(w)) + E(w)\right) \tag{41}$$

The result of Nagai's [17] and Piri's [35] calculations are compared as shown in Figure 7, which both show the coupling coefficients as a monotonic decreasing function of distance. At a large distance, the coupling coefficient is zero, and at the closed position, the mutual inductance has to be consistent with the self-inductance. The other observation which is in consistent with the findings from the previous investigators is that larger the coil diameter, the larger the coupling coefficient at the same distance g.

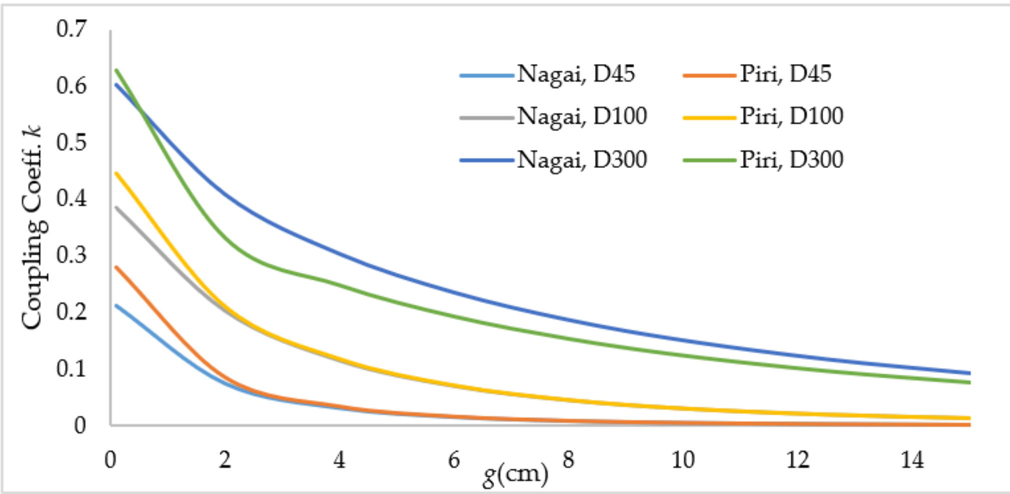

Figure 7. Coupling coefficient k versus gap g with different D (mm) under N = 14, and d = 1.3 mm conditions.

4. Experimental Verification

The WPT experiment was conducted using the Class E PA, as shown in Figure 3. The GaN HEMT transistor is used to drive the Class E PA which was designed and fabricated by a Compound Semiconductor Device (CSD) at the research Lab at The National Yang Ming Chiao Tung University. The GaN transistor is a normally on device; thus, the charge pump circuit design between the high current gate driver and the transistor is necessary [27–31]. The parameters and characteristic curves of the GaN transistor are shown in Figure 8. The transistor characteristics includes the threshold voltage V_{th} = −9 V, the continuous drain current I_D = 35 A, the drain to source breakdown voltage V_{BD} > 1 kV, and the on-resistance $R_{DS(on)}$ = 120 mΩ. Parasitic capacitances versus drains to source the voltage v_{DS} of the GaN transistor that were measured by a semiconductor parameter analyzer Keysight B1500A are shown in Figure 8c. It indicates a five-fold capacitance difference during the period of switch off, which is smaller than that of a traditional silicon based Metal-Oxide-Semiconductor Field-Effect Transistor (MOSFET).

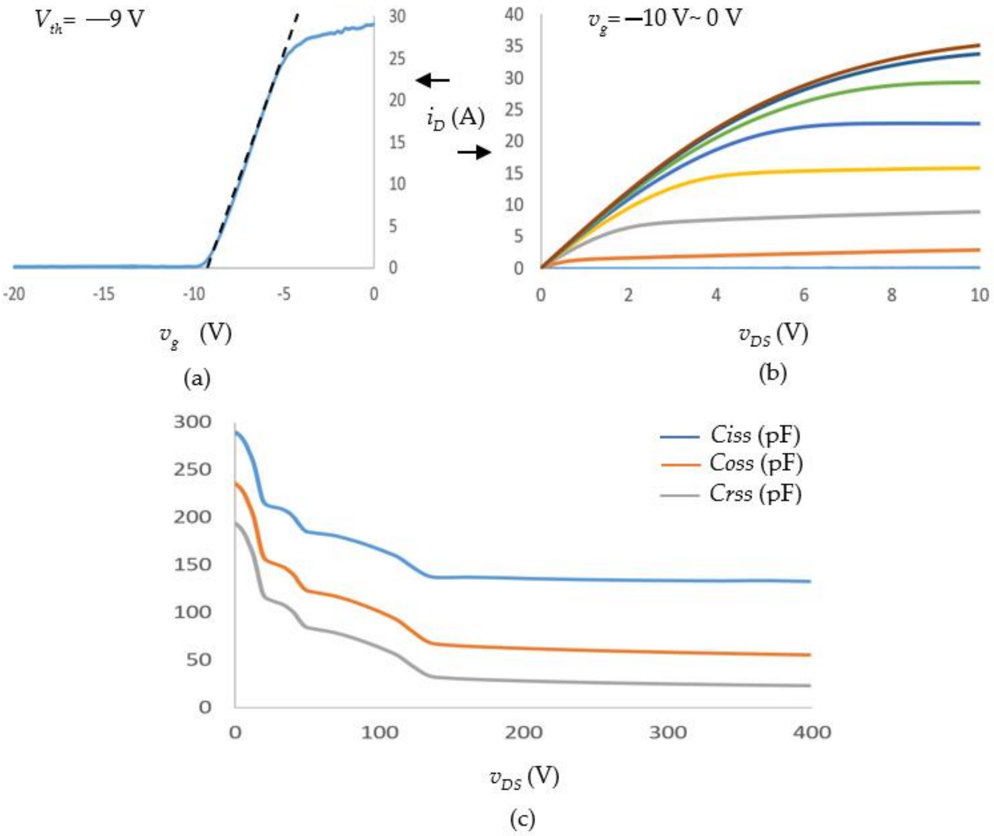

Figure 8. GaN Transistor parameters (**a**) i_D versus v_g curve, (**b**) i_D versus v_{DS} curve, (**c**) parasitic capacitance versus v_{DS} curve.

The capacitor on the secondary end must withstand nearly 1 kV, and we expect certain nonlinear distortion to be seen in the experiments. The experimental schematic view and setup are shown in Figure 9a,b, respectively, where two hollow tube coils made by copper are used as transmitters and receivers that are connected to class E PA and load resistor R_0. The input power is read from the power supply CHROMA 62012P-600-8. The receiver RMS voltage value is taken from the differential voltage probe SI-9002 and the oscilloscope Tektronix MDO3054. The current probe is not applicable for the PRU measurement, as the current probe will be affected by magnetism and yield an excessive current value. Figure 9c depicts the implementation of the class E PA on a printed circuit board (PCB) with dimensions of 5 cm by 6 cm, which was utilized in the experiment. The PRUs are connected in parallel with the power resistor of 10 kΩ, as shown in Figure 9d,e. Two kinds of power resistors were used in the experiment. Due to the different fabrication process, the wire wound one will have a higher parasitic inductance than the film one. The parasitic inductances of two different kinds of resistors were 300 µH and 40 nH, which were measured using a GWINSTEK LCR819 RLC meter. This is due to the skin effect, whereby the tendency of an AC current to become distributed within a conductor is such that the current density is largest near the surface of the conductor and decreases exponentially with greater depths in the conductor. Table 2 lists the parameters and specifications of class E PA and the hollow tube used in the experiment.

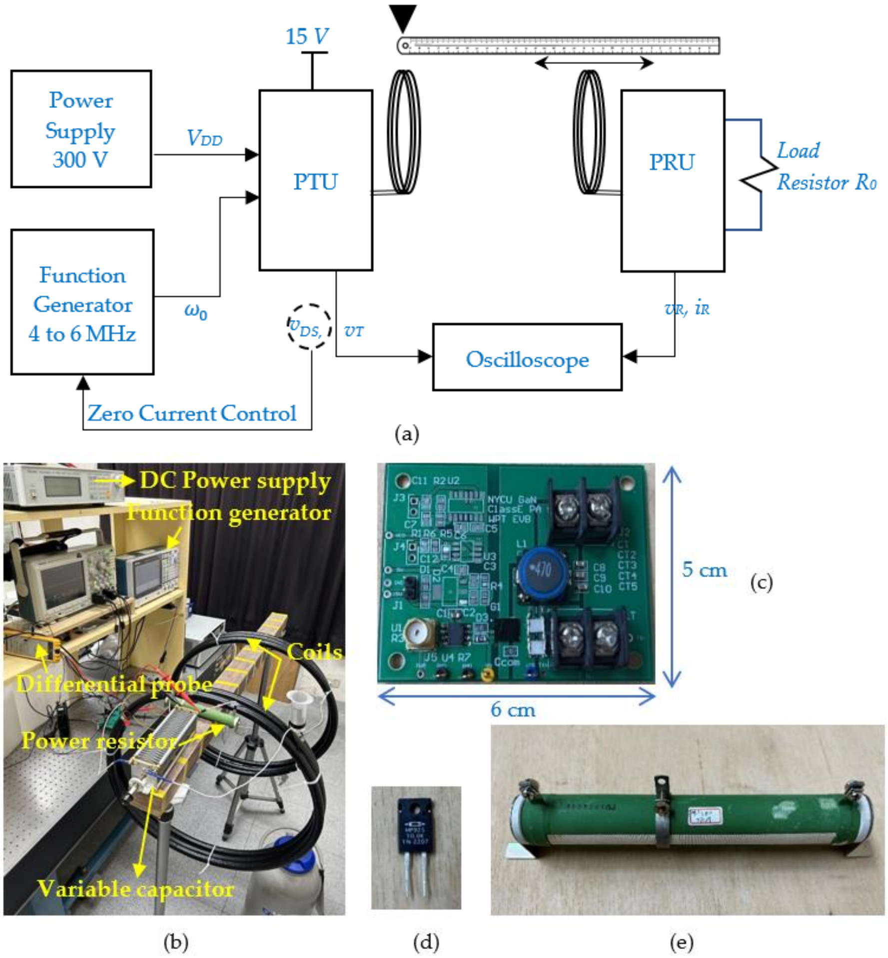

Figure 9. (**a**) Schematic view of the experiment, (**b**) experiment setup, (**c**,**d**) class E PA PTU according to Figure 3, (**d**) wire wound power resistor, (**e**) film power resistor.

Table 2. Experiment Parameter.

Class E PA			Units
Gate driver	UCC27614 (TI)		
Switch M_1	GaN HEMT (NYCU)		
Inductance L_1	47		µH
Capacitance C_T	200		pF
Coils	**PTU**	**PRU**	
Inductance L_T, L_R	10	9.6	µH
Windings N	2.75	2.75	Turns
Coil Diameter D	72	72	cm
Coil length l	7.8	7.8	cm
Tube Diameter d	2.8	2.8	cm
Tube Thickness	0.8	0.8	mm
Capacitance C_R		137	pF
Coil Resistance $R_{R,c}$		0.08	Ohm

4.1. Maximum Voltage Gain and Coupling Coefficient

The measurement results from the experiments show that the maximum voltage gain $|G_{V,1}|$ is increasing along with the distance gap g and R_0, which is demonstrated in Figure 10a. The maximum voltage gain $|G_{V,1}|$ is reduced when the parallel quality factor $Q_{p,0}$ is increased, Equation (24). The actual products of voltage gain and the coupling coefficient can match the theoretical values with 30% max. error. The error between the actual product and the ideal constant reduces as the diameter of the transformer increases.

The maximum voltage gain implies the maximum power efficiency because PDL is the square voltage divided by the load resistance (kΩ) on PRU. The higher the power received by PRU, the higher the PTE is. From Figure 10b, which shows the PTE% via different distances and load resistances, we can observe that the maximum voltage gain points are forming the ridge of the PTE surface. The two sides of the ridge (or saddle point) are with different slope gradients due to their PDL differences, which will be discussed in a later section.

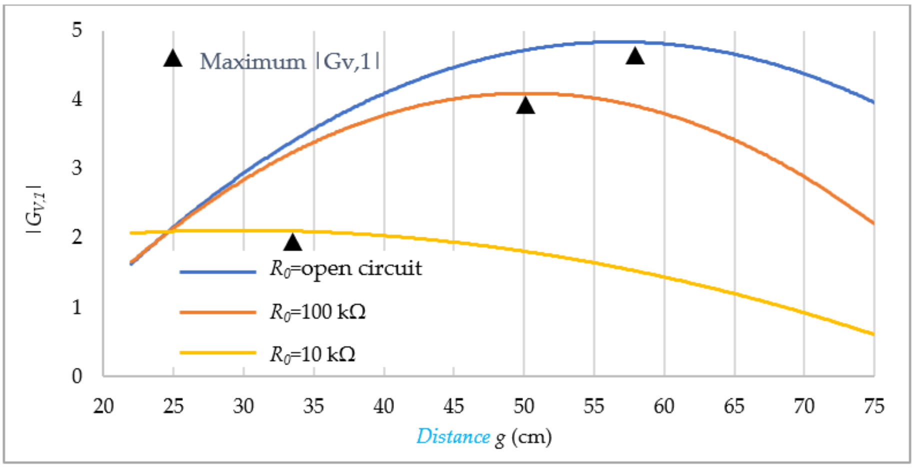

(**a**)

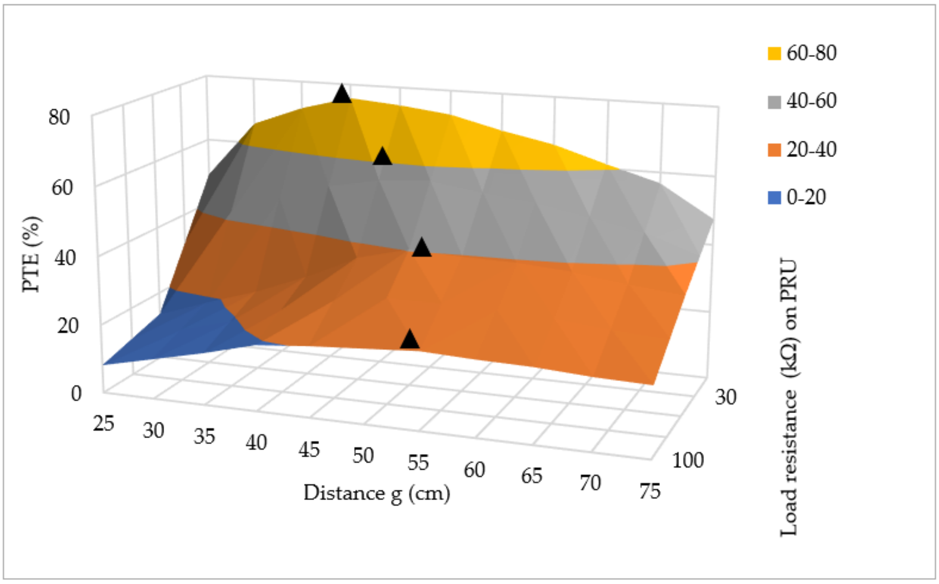

(**b**)

Figure 10. *Cont.*

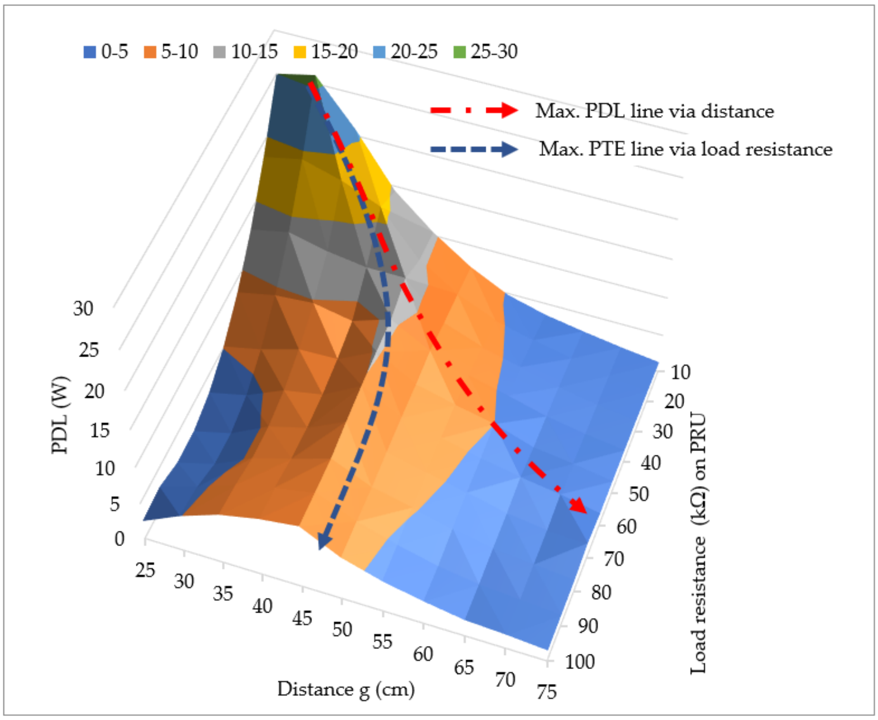

(**c**)

Figure 10. Measurement results of the resonant WPT under zero current switching; (**a**) v_T, v_R and PDL versus V_{DD}; and (**b**) PTE for different distances and loads; and (**c**) Max. PDL and PDE for different distances and load resistances.

In Figure 10c, we show the experimental results with interpolation on the PDL via different distances and load resistances. In addition to the maximum PTE line in the black dot line via a different load resistance R_0 corresponding to Figure 10b, we can find the other ridge from the view of distance g in cm. The distance is directly related to the coupling coefficient as well as the maximum voltage gain. The maximum PDL line in the red center-dash line along the same distance is a function of the load resistance R_0, which can also be found according to Equation (25). Along the maximum PDL line is the best load resistance to receive the maximum power for a given distance. In order to find the maximum PDL line experimentally, we may apply the hill climbing method to adjust the load resistance R_0 in order to reach the maximum power. The load resistance adjustment requires certain dc chopper or DC-DC converter controls, as stated previously.

As shown in Figure 11, the voltage gain $|G_{V,1}|$ derived in Equation (14) is practically a function of V_{DD}. In order to understand the maximum power that can be transferred via a single GaN HEMT-based class E PA module, we fixed the switching frequency to 4 MHz, the duty to 50%, the distance to 35 cm, and measured the voltage gain and the PDL. The adjustable capacitor can only endure 1 kV and the waveform is distorted after V_{DD} = 80 V. When V_{DD} = 85 V, the PDL is 45 W and the V_R reaches 1.27 kV. The PDL is calculated from (25) with the output resistance R_0 connected to 10 kΩ. There are two kinds of resistors used in different power levels, and the film resistor MP925 made by Caddock in the TO-220 package cannot withstand a received power of over 25 W. Thus, it is substituted by the wirewound one, which is capable of hundreds of watts of power. However, the extra parasitic inductance may have an influence on the reception of practical power and the resonant quality factor. The PDL monotonically increases with the input voltage, and the voltage on the PRU can be as high as 1.27 kV when the input voltage is at 85 V. Class E PA oscillates DC voltage V_{DD} into the sinusoidal PTU coil voltage output with V_T as high as 3.5 times on average [27]. Hence, when the V_{DD} is 150 V, the GaN HEMT is subjected to a turn-off drain-source voltage $V_{DS} \approx$ max. The V_T is around 1 kV. According to the interpolation data shown in Figure 11, when the V_{DD} is 150 V, the power delivery is 150 W. Our GaN HEMT is capable of enduring the breakdown voltage above 1 kV, which allows for the delivery of 150 W to the PRU when the load resistance is 10 kΩ. The 150 VDC can be easily acquired from the 110 VAC through the AC/DC converter at home, and this is a main reason why the class E amplifier is used.

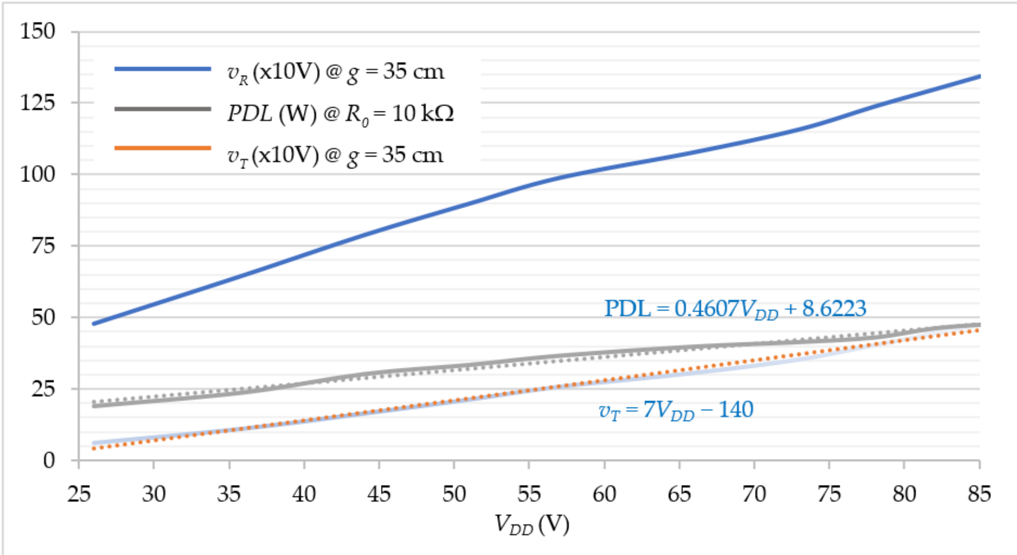

Figure 11. v_T, v_R and PDL versus input DC voltage V_{DD}.

4.2. Power Transfer Efficiency

The experiments with non-ideal conditions such as the external resistor R_0 in parallel with the capacitor C_R will increase the parallel quality factor Q_p. The conventional mutual inductance model supporting the inductive power transfer is known as the strongly coupled WPT, and can only be effective in delivering power for short distances. The resonant WPT is also known as the loosely coupled wireless power transfer that can be used to transfer power over a long distance. The coupling coefficient decreases as the distance between coils increases, as shown in Figure 7. The PDL is a function of the switching frequency for the WPT. The phase shift between the PTU and PRU, stated in Equation (18), can be used to control the WPT delivering power at longer distances. The experiments show that the phase shifts for those PDL peaks that occurred in the short distance are nearly zero degrees, hence they are the inductive power. The phase shifts for those PDL peaks that occurred at a long distance are nearly 90, and can be regarded as resonant power. The inductive power transfer is limited by conventional transformer theory so that the voltage gain is unified when the turn ratio between windings is one. As a result, there is no phase difference at very close WPT. In our experiment, the phase of two coils is controlled within 45°, which satisfies the optimal k condition in (19).

Figure 12 shows one of our experiment results via distance, in which the PTE is compared to those reported in Table 1 with their maximum PTE. The results from [5,19,32] are sub-MHz resonant WPT when rest of them [17,18,33], including this work, are resonant in the frequency above 2 MHz. It is theoretically possible that the higher the resonant frequency, the longer the distance that the wireless power can be transferred. Therefore, the work shown in [19] is a special case due to its special, strongly coupled resonance mechanism. Compared to the results shown in [17,18,33], our result demonstrates the highest PTE and possibly also the largest PDL. The work of [18] can deliver wireless power to a greater distance than this study, whose actual PDL is not reported. Figure 13 shows our experimental results with increasing input voltage V_{DD}. The PDL monotonically increases and the PTE monotonically decays with the increasing input power P_{in}. We artificially mapped the comparisons among all results according to their efficiency reported to the input power of 100 W. The research work in [5] has the highest PDL, albeit at a short distance. Our analysis of the experiment data including both the PDL and the PTE calculation are according to the power resistor MP925 without any inductance; therefore, the measured power is the actual power delivered to the load resistance. Figure 14 shows the waveforms of v_{GS}, v_{DS}, v_T and v_R, which demonstrates that our class E amplifier is working in its zero- current switching (ZCS) phase. The ZCS ensures the lowest transistor switching loss, and thus the best efficiency is obtained. It can also be seen that the voltage v_R is in its perfect sinusoidal resonance.

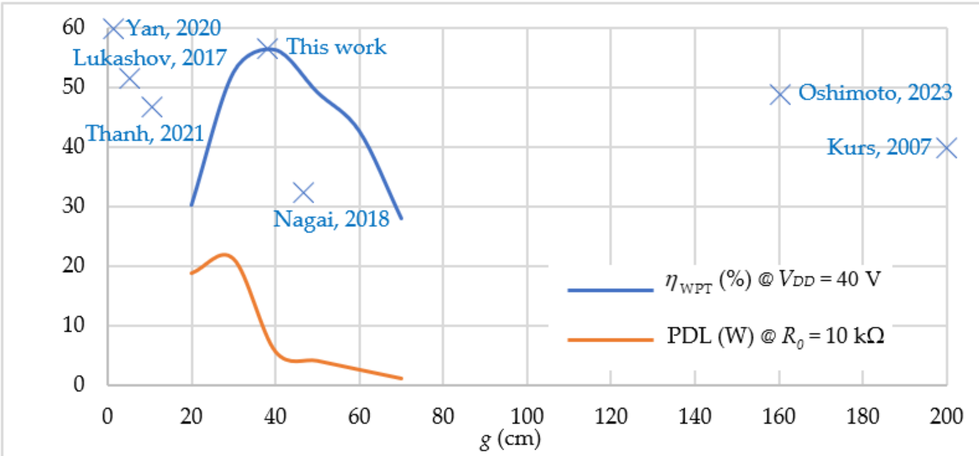

Figure 12. η_{WPT} and PDL versus different distance gap g [5,17–19,32,33].

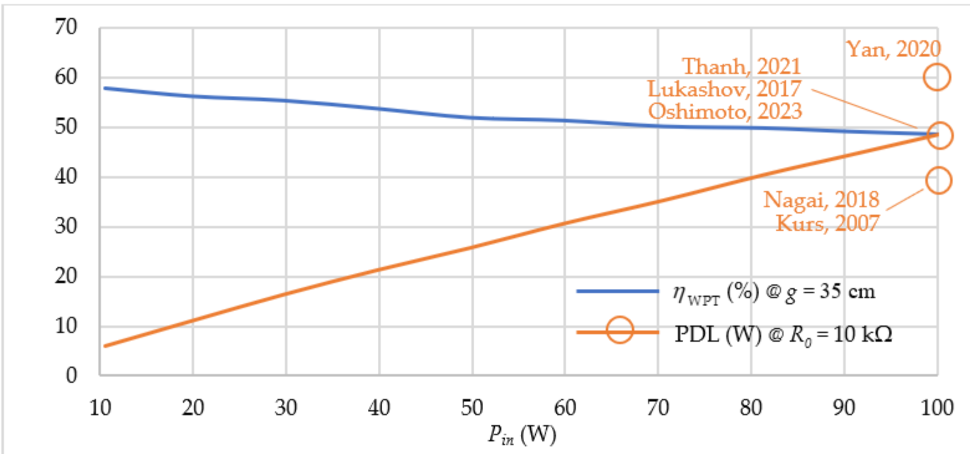

Figure 13. PDL and η_{WPT} versus P_{in} [5,17–19,32,33].

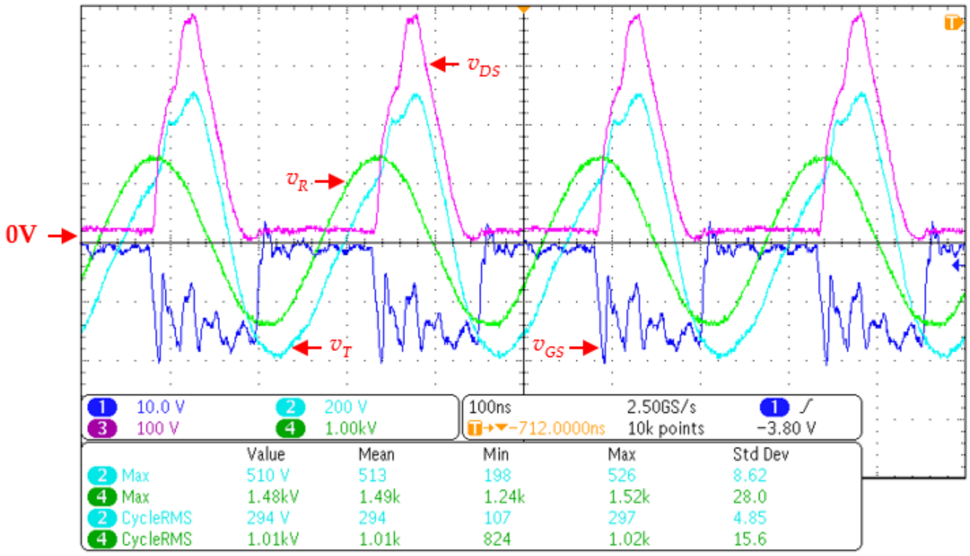

Figure 14. Oscilloscope waveform under 45° phase difference and the achieved maximum PDL at a distance of 35 cm.

5. Conclusions

This paper provides the schemes for implementing a long-distance WPT system, which is verified by Class E PA and operated in the MHz frequency. A normally-on GaN device is used to drive high transmitter voltage at radio frequency. The coil inductor and WPT system are analyzed in the paper in detail. Meanwhile, a pair of hollow copper tubes were designed and used to verify the constant product of voltage gain and coupling coefficient at resonance. The experimental results show that the voltage gain and transferred power can be increased by either reducing the coil resistance of the receiver or increasing the coupling coefficient, and the transfer distance can be increased by matching the parallel quality factor and the coupling coefficient. Having the smallest possible parallel quality factor Q_p is the key to increasing both the maximum voltage gain and the power transfer distance. High load resistance and low coil resistance are both beneficial in decreasing the parallel quality factor Q_p. However, the high load resistance on the PRU will reduce the rate of harvesting power on the PRU. The load resistance tuning can be used in the maximum power point tracking when the PRU is moving. When we need to increase the power transfer for a fixed distance, we then need to reduce the coil resistance to directly reduce the parallel quality factor Q_p according to Equation (13) due to a fixed switching (or resonant) frequency and a fixed PRU coil. There are many ways to reduce the coil resistance, for example by the cooling of the coil to its low resistance, as is done in outer space. The other way of lowering the parallel quality factor Q_p is to reduce the resonant frequency so that we may have a larger PRU capacitor storing and converting the magnetic power from the LC tank of the PRU. The findings are becoming clearer for the utilization of large diameter coils or superconductor materials, which also make a significant contribution to long-distance WPT systems, with potential applications in various industries such as healthcare and consumer electronics. In a future work, we will proceed on to the coil design to achieve the kW requirements.

Author Contributions: Conceptualization, W.-H.C.; methodology, C.-C.W.; software, W.-H.C.; validation, C.-Y.L. and C.-C.W.; formal analysis, C.-Y.L., Y.-T.S. and C.-C.W.; resources, E.-Y.C.; writing—original draft preparation, L.-C.T. and W.-H.C.; writing—review and editing C.-C.W. and C.-Y.L.; visualization, W.-H.C.; experiments, L.-C.T., Y.-T.S. and C.-Y.L.; supervision, E.-Y.C.; project administration, E.-Y.C.; funding acquisition, E.-Y.C. and W.-H.C. All authors have read and agreed to the published version of the manuscript.

Funding: This research was funded by National Science and Technology Council (NSTC) and Ministry of Science and Technology (MOST), R.O.C., grant number NSTC 111-2622-8-A49-018-SB and MOST 110-2622-8-007-019.

Institutional Review Board Statement: Not applicable.

Informed Consent Statement: Not applicable.

Data Availability Statement: Data sharing not applicable.

Acknowledgments: The authors also thank You-Chen Weng of the CSD Lab for fabricating the D-Mode MIS-HEMT chips, and the IMLab graduate students for their help with the experimental setup.

Conflicts of Interest: The authors declare that they have no conflict of interest.

Nomenclature

Symbol	**Abbreviation**
$L_{T,s}$	the self-inductance of the PTU
L_m	mutual inductance
$L_{R,l}$	the leakage inductance of the PRU
v_T	the voltage across the transmitter coil
$v_{T,i}$	transfer voltage of the PTU
$v_{R,i}$	the induced receiver voltage
v_R	the voltage across the receiver coil
i_T	current flowing through the transmitter coil
$i_{R,i}$	current flowing through the receiver coil
N_T	turns of the transmitter coil
N_R	turns of the receiver coil
a	the turn ratio of N_T and N_R
R_T	the reluctance of the transmitter coil
$R_{R,c}$	the coil resistance on the winding on the receiver side
Z_R	receiver impedance
Z_o	the load impedance
C_R	the resonant capacitor of the PRU
A	the cross section area of the inductor of the PTU
B	flux density
φ_m	magnetization flux
φ_i	induction flux
φ_s	self-induction flux
k	coupling coefficient
f_0	the natural frequency
L_T	transmitter inductance
L_R	receiver inductance
Q_p	the parallel quality factor without considering load
ε	the mismatch of the inductance
ψ	the correction factor
$G_{V,1}$	the voltage gain when the transmitter frquency matchs the receiver
$G_{V,\psi}$	the voltage gain when the transmitter frquency mismatchs the receiver
$f(k)$	the monotonic increasing function with the coupling coefficient k
$Q_{p,0}$	the parallel quality factor with considering load
$P_{0,RMS}$	root mean square received power
δ	duty ratio of class E PA control signal
M_1	switch of class E PA
v_{GS}	gate to source voltage of switch
C_{DS}	drain to source capacitance of switch
v_{DS}	drain to source voltage of switch
P_{in}	class E PA power input
i_1	class E PA input current
V_{DD}	class E PA input voltage
L_1	choke inductor of class E PA

C_T	the resonant capacitor of PTU
g	distance gap between two coils
l	the coil legth
D	the coil diameter
l_w	the wire length of coil
L_{ext}	the external inductance
δ_i	The coil skin depth
$Ciss$	The GaN HEMT input capacitance
$Coss$	The GaN HEMT output capacitance
$Crss$	The GaN HEMT reverse tansfer capacitance

References

1. Jiang, C.; Chau, K.T.; Liu, C.; Lee, C.H.T. An Overview of Resonant Circuits for Wireless Power Transfer. *Energies* **2017**, *10*, 894. [CrossRef]
2. Sidiku, M.B.; Eronu, E.M.; Ashigwuike, E.C. A review on wireless power transfer: Concepts, implementations, challenges, and mitigation scheme. *Niger. J. Technol.* **2020**, *39*, 1206–1215. [CrossRef]
3. Sun, L.; Ma, D.; Tang, H. A review of recent trends in wireless power transfer technology and its applications in electric vehicle wireless charging. *Renew. Sustain. Energy Rev.* **2018**, *91*, 490–503. [CrossRef]
4. Ahmad, A.; Alam, M.S.; Chabaan, R. A Comprehensive Review of Wireless Charging Technologies for Electric Vehicles. *IEEE Trans. Transp. Electrif.* **2018**, *4*, 38–63. [CrossRef]
5. Yan, Y.; Shi, W.; Zhang, X. Design of UAV wireless power transmission system based on coupling coil structure optimization. *EURASIP J. Wirel. Commun. Netw.* **2020**, *2020*, 67. [CrossRef]
6. Khan, S.R.; Pavuluri, S.K.; Cummins, G.; Desmulliez, M. Wireless Power Transfer Techniques for Implantable Medical Devices: A Review. *Sensors* **2020**, *20*, 3487. [CrossRef]
7. Weng, Y.C.; Wu, C.C.; Chang, E.Y.; Chieng, W.H. Minimum Power Input Control for Class-E Amplifier Using Depletion-Mode Gallium Nitride High Electron Mobility Transistor. *Energies* **2021**, *14*, 2302. [CrossRef]
8. Gilabert-Palmer, D.; Sanchis-Kilders, E.; Esteve, V.; Ferreres, A.; Ejea, J.B.; Maset, E.; Jordn, J.; Dede, E. Measuring coupling coefficient of windings with dissimilar turns' number or tight coupling using resonance. *IEEE Trans. Power Electron.* **2018**, *33*, 9790–9802. [CrossRef]
9. Zaoskoufis, K.; Tatakis, E.C. The coupling coefficient impact on the dc voltage gain of the passive clamp coupled inductor boost converter. In Proceedings of the 2018 20th European Conference on Power Electronics and Applications (EPE'18 ECCE Europe), Riga, Latvia, 17–21 September 2018; IEEE: Piscataway, NJ, USA, 2018; pp. P.1–P.9.
10. Zaoskoufis, K.; Tatakis, E.C. A Thorough Analysis for the Impact of the Coupling Coefficient on the Behavior of the Coupled Inductor High Step-Up Converters. *IEEE Trans. Power Electron.* **2020**, *35*, 8287–8302. [CrossRef]
11. Ayachit, A.; Kazimierczuk, M.K. Transfer functions of a transformer at different values of coupling coefficient. *IET Circuits Devices Syst.* **2016**, *10*, 337–348. [CrossRef]
12. Li, Y.; Zhang, H.; Liang, X.; Huang, B. Event-Triggered-Based Distributed Cooperative Energy Management for Multienergy Systems. *IEEE Trans. Ind. Inform.* **2019**, *15*, 2008–2022. [CrossRef]
13. Hou, X.; Wang, Z.; Su, Y.; Liu, Z.; Deng, Z. A Dual-Frequency Dual-Load Multirelay Magnetic Coupling Wireless Power Transfer System Using Shared Power Channel. *IEEE Trans. Power Electron.* **2022**, *37*, 15717–15727. [CrossRef]
14. Li, X.; Hu, J.; Wang, H.; Dai, X.; Sun, Y. A New Coupling Structure and Position Detection Method for Segmented Control Dynamic Wireless Power Transfer Systems. *IEEE Trans. Power Electron.* **2020**, *35*, 6741–6745. [CrossRef]
15. Mendes Duarte, R.; Klaric Felic, G. Analysis of the coupling coefficient in inductive energy transfer systems. *Act. Passiv. Electron. Compon.* **2014**, *2014*, 951624. [CrossRef]
16. Chabalko, M.J.; Sample, A.P. Resonant cavity mode enabled wireless power transfer. *Appl. Phys. Lett.* **2014**, *105*, 243902. [CrossRef]
17. Nagai, C.; Inukai, K.; Kobayashi, M.; Tanaka, T.; Abumi, K.; Imura, T.; Hori, Y. Scaling law of coupling coefficient and coil size in wireless power transfer design via magnetic coupling. *Electr. Eng. Jpn.* **2018**, *202*, 21–30. [CrossRef]
18. Oshimoto, N.; Sakuma, K.; Sekiya, N. Improvement in Power Transmission Efficiency of Wireless Power Transfer System Using Superconducting Intermediate Coil. *IEEE Trans. Appl. Supercond.* **2023**, *33*, 1501004. [CrossRef]
19. Kurs, A.; Karalis, A.; Moffatt, R.; Joannopoulos, J.D.; Fisher, P.; Soljačić, M. Wireless power transfer via strongly coupled magnetic resonances. *Science* **2007**, *317*, 83–86. [CrossRef]
20. Ziegler, C.; Weber, S.; Heiland, G.; Kraus, D. Influences of WPT-Coil Losses and Coupling Coefficient on the Resonance Circuits of Wireless Power Transfer Systems. In Proceedings of the PCIM Europe 2017, International Exhibition and Conference for Power Electronics, Intelligent Motion, Renewable Energy and Energy Management, Frankfurt, Germany, 16–18 May 2017; pp. 1–7.
21. Zhang, J.; Cheng, C. Analysis and Optimization of Three-Resonator Wireless Power Transfer System for Predetermined-Goals Wireless Power Transmission. *Energies* **2016**, *9*, 274. [CrossRef]
22. Gu, P.; Wang, Y.; Mai, J.; Yao, Y.; Gao, S.; Huang, S.; Xu, D. A Three-Stage-Five-Coil IPT System Based on Cylindrical Solenoid Coupler Applied to State Detection Equipment of HV Device. *IEEE Trans. Power Electron.* **2022**, *37*, 2382–2393. [CrossRef]

23. Huang, X.; Yu, Z.; Dou, Y.; Lin, S.; Ouyang, Z.; Andersen, M.A.E. Load-Independent Push–Pull Class E 2 Topology with Coupled Inductors for MHz-WPT Applications. *IEEE Trans. Power Electron.* **2022**, *37*, 8726–8737. [CrossRef]
24. He, L.; Huang, X.; Cheng, B. Robust Class E2 Wireless Power Transfer System Based on Parity–Time Symmetry. *IEEE Trans. Power Electron.* **2023**, *38*, 4279–4288. [CrossRef]
25. Sekiya, H.; Tokano, K.; Zhu, W.; Komiyama, Y.; Nguyen, K. Design Procedure of Load-Independent Class-E WPT Systems and Its Application in Robot Arm. *IEEE Trans. Ind. Electron.* **2022**, *70*, 10014–10023. [CrossRef]
26. Issi, F.; Kaplan, O. Design and application of wireless power transfer using Class-E inverter based on Adaptive Impedance-Matching Network. *ISA Trans.* **2022**, *126*, 415–427. [CrossRef] [PubMed]
27. Liu, C.-Y.; Wang, G.-B.; Wu, C.-C.; Chang, E.Y.; Cheng, S.; Chieng, W.-H. Derivation of the Resonance Mechanism for Wireless Power Transfer Using Class-E Amplifier. *Energies* **2021**, *14*, 632. [CrossRef]
28. Wu, C.-C.; Liu, C.-Y.; Anand, S.; Chieng, W.-H.; Chang, E.-Y.; Sarkar, A. Comparisons on Different Innovative Cascode GaN HEMT E-Mode Power Modules and Their Efficiencies on the Flyback Converter. *Energies* **2021**, *14*, 5966. [CrossRef]
29. Wu, C.-C.; Liu, C.-Y.; Wang, G.-B.; Shieh, Y.-T.; Chieng, W.-H.; Chang, E.Y. A New GaN-Based Device, P-Cascode GaN HEMT, and Its Synchronous Buck Converter Circuit Realization. *Energies* **2021**, *14*, 3477. [CrossRef]
30. Kumar, R.; Wu, C.-C.; Liu, C.-Y.; Hsiao, Y.-L.; Chieng, W.-H.; Chang, E.-Y. Discontinuous Current Mode Modeling and Zero Current Switching of Flyback Converter. *Energies* **2021**, *14*, 5996. [CrossRef]
31. Tang, L.-C.; Jeng, S.-L.; Chang, E.-Y.; Chieng, W.-H. Variable-Frequency Pulse Width Modulation Circuits for Resonant Wireless Power Transfer. *Energies* **2021**, *14*, 3656. [CrossRef]
32. Lukashov, S.V. A Self-Tuning 100-Watt Wireless Power Transfer System. Ph.D. Thesis, Massachusetts Institute of Technology, Cambridge, MA, USA, 2017.
33. Thanh, S.P.; Thao, D.N.; Bui, S.T.; Bui, X.K.; Thu, T.H.; Quang, M.N.; Le, T.H.H.; Vu, D.L. Optimal frequency for magnetic resonant wireless power transfer in conducting medium. *Sci. Rep.* **2021**, *11*, 18690. [CrossRef]
34. De Oliveira Barros Luna, B.E.; Jacobina, C.B.; Oliveira, A.C. Internal Energy Balance of a Modular Multilevel Cascade Converter Based on Chopper-Cells with Distributed Energy Resources for Grid-Connected Photovoltaic Systems. *IEEE Trans. Ind. Appl.* **2023**, *59*, 1935–1943. [CrossRef]
35. Piri, M.; Jaros, V.; Frivaldsky, M. Verification of a mutual inductance calculation between two helical coils. In Proceedings of the 2015 16th International Scientific Conference on Electric Power Engineering (EPE), Kouty nad Desnou, Czech Republic, 20–22 May 2015; pp. 712–717.
36. Knight, D.W. An Introduction to the Art of Solenoid Inductance Calculation with Emphasis on Radio-Frequency Applications. Version 0.20. 4 February 2016. Available online: https://g3ynh.info/zdocs/magnetics/Solenoids.pdf (accessed on 2 March 2023).